Few-Body Syst (2023) 64:58
https://doi.org/10.1007/s00601-023-01842-9

Huey-Wen Lin

Overview of Lattice Results for Hadron Structure

Received: 15 April 2023 / Accepted: 14 June 2023

Abstract In recent years, there have been many advances in the hadron structure using lattice QCD. There have also been improvements in hadron charges, form factors and moments, with the continuum-physical limit being taken, removing all lattice artifacts. There was a breakthrough in calculating the Bjorken-x dependence of PDFs in lattice QCD by using large-momentum effective theory and similar frameworks. This breakthrough has led to the emergence and rapid development of direct calculations of Bjorken-x dependent structure. In this talk, I will review recent progress made in lattice QCD and future challenges.

1 A Brief Introduction to Lattice QCD

Lattice QCD is a theoretical tool that allows us to study the nonperturbative regime of QCD directly with full systematic control. The approach is based on regularizing QCD on a finite four-dimensional Euclidean spacetime lattice and is often studied using numerical computations of QCD correlation functions in the path-integral formalism using national-scale supercomputers. As in continuum QCD, we calculate an observable of interest through a path integral:

$$\langle 0|O(\overline{\psi},\psi,A)|0\rangle = \frac{1}{Z}\int [dA][d\overline{\psi}][d\psi]O(\overline{\psi},\psi,A)e^{i\int dx^4\mathcal{L}_{\rm QCD}(\overline{\psi},\psi,A)}, \tag{1}$$

where $\mathcal{L}_{\rm QCD}$ is the sum of the pure-gauge and fermion Lagrangian, O is the operator that gives the correct quantum numbers for physical observable, and Z is the partition function of the spacetime integral of the QCD Lagrangian. It is straightforward to carry out this path integral numerically within a finite spacetime volume and under an ultraviolet cutoff (the lattice spacing a). To make contact with experimental data, the numerical results are extrapolated to the continuum (with lattice spacing $a \to 0$) and infinite-volume ($L \to \infty$) limits. When the calculation is done using heavier-than-physical quark masses (to save computational time), one also has to take the $m_q \to m_q^{\rm phys}$ limit. A recent overview can be found in Ref. [1]. In the past decade, there has been significant progress in the development of efficient algorithms for the generation of ensembles of gauge-field configurations and tools for extracting relevant information from lattice-QCD correlation functions. Lattice-QCD calculations have reached a level where they not only complement, but also guide current and forthcoming experimental programs. Further details, we refer readers to a recent lecture note in Ref. [1]

H.-W. Lin (✉)
Department of Physics and Astronomy & Department of Computational Mathematics, Science and Engineering, Michigan State University, East Lansing, MI 48824, USA
E-mail: hwlin@pa.msu.edu

Published online: 05 July 2023

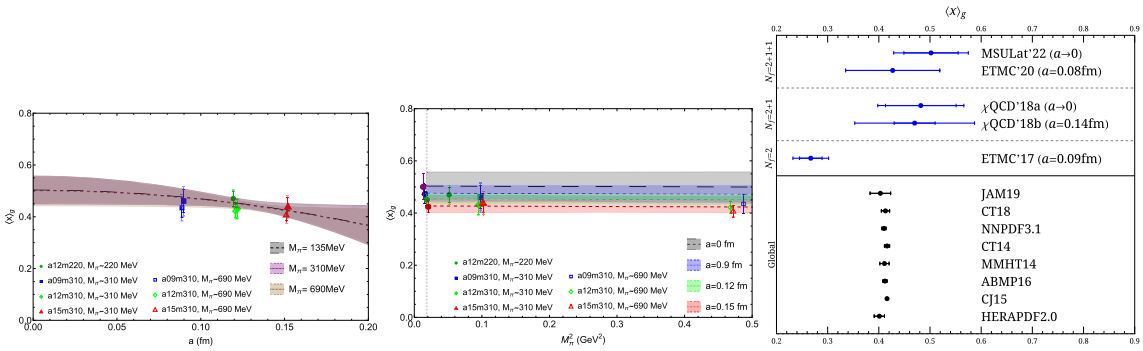

Fig. 1 The renormalized gluon momentum fraction $\langle x \rangle_g^{\overline{\rm MS}}$ obtained from each ensemble along with the physical-continuum extrapolation as functions of lattice spacing a (left) and pion mass M_π^2 (middle). Each data point in the plot has two errors: the darker inner bar indicates the statistical error, while the lighter outer bar includes combined errors from both the statistical and renormalization error. The vertical dashed line in the right plot goes through $M_\pi^2 = (0.135\ \text{GeV})^2$, and the different color points near this line represent the extrapolated values at different lattice spacings a at physical pion mass. To increase visibility, we plot the $M_\pi \in \{220, 310\}$-MeV points shifted by $+0.001$ fm in the left plot. The reconstructed fit bands at selected $M_\pi \in \{135, 310, 690\}$ MeV as functions of a and at selected $a \in \{0, 0.09, 0.12, 0.15\}$ fm as functions of M_π are also shown in the left- and right-side plots, respectively. (right) Comparisons of lattice-QCD and global fit determinations of the gluon moments of unpolarized PDFs at $\mu = 2$ GeV. On the lattice side, we only show those results at or extrapolated to physical pion mass by this work (MSULat'22), ETMC'20 [4], χQCD'18a[5], χQCD'18b[6], and ETMC'17 [7], compared with global fit results from JAM19 [8], CT18 [9], NNPDF3.1 [10], CT14 [11], MMHT14 [12], ABMP16 [13], CJ15 [14] and HERAPDF2.0 [15] analyses. Some lattice-QCD calculations include systematic errors and some do not; we refer readers to Table 1 for more details on the difference in the errors. Overall, the lattice calculations prefer higher central values of the gluon momentum fraction than the global fits. Figures taken from Ref. [16]

2 Nucleon Structure with Controlled Systematics

The progress of lattice hadron calculations has long been limited by computational resources, but recent advances in both algorithms and a worldwide investment in pursuing exascale computing has led to exciting progress in LQCD calculations. Many nucleon structure calculations are done directly at the physical pion mass, some with multiple lattice spacings. Due to the page limit, we refer interested readers these recent reviews for more details on lattice moments [2,3]. Reference [2] outlines a lattice-community rating system for lattice nucleon quantities; the goal is to assess the quality of papers from different collaborations using a simple rating scheme so that non-lattice physicists can understand possible reasons for discrepancy among lattice results, indicating whether there is tension among them or if some calculations are missing important systematics. Reference [1] gives a recent summary; in this proceeding, we give a few examples since the review.

The gluon structure is notoriously difficult to calculate on the lattice due to the signal-to-noise problem. Recent work by MSULat group [16] calculated renormalized gluon momentum fractions $\langle x \rangle_g^{\overline{\rm MS}}$ at three lattice spacings and three pion masses as shown in Fig. 1. The points in Fig. 1 have two kinds of errorbars; the darker smaller bars include only the statistical error for the gluon momentum fraction, while the lighter larger bars include both the statistical errors and the errors from the gluon NPR factor. The renormalized $\langle x \rangle_g^{\overline{\rm MS}}$ is extrapolated in M_π and a to the physical-continuum extrapolation to the physical pion mass $M_\pi^{\rm phys} = 135$ MeV and continuum limit $a = 0$ The physical-continuum limit gluon momentum fraction $\langle x \rangle_g^{\overline{\rm MS},\rm cont}$ fit result is 0.502(53). The reconstructed fit bands at selected $M_\pi \in \{135, 310, 690\}$ MeV as functions of a are shown in the left plot of Fig. 1. There is a slight trend toward higher gluon momentum fractions as one approaches the physical pion mass. The $M_\pi = 690$ MeV band deviates from the other two bands, while the $M_\pi = 135$ and 310 MeV bands almost coincide. One can also see that the fit form well describes the data since these bands go through the $M_\pi = 220$- and 310-MeV data points. The middle plot of Fig. 1 shows the reconstructed results at $a \in \{0, 0.09, 0.12, 0.15\}$ fm as functions of M_π with each color band representing different lattice spacings agrees well with the same-color data points. The right-hand side of Fig. 1 shows a comparison with all prior dynamical lattice work and global fits. The majority of nucleon gluon momentum fractions $\langle x \rangle_g$ from lattice dynamical calculations were done using a single lattice spacing. These results range from 0.4 to 0.55 for the most recent calculations (except the ETMC16 and ETMC17 results) and have statistical errors varying from 5–20%. Overall, there is good consistency with lattice determinations from the last four years. The lattice results currently are much larger than with those from global fits, with central values closer to 0.5, rather than

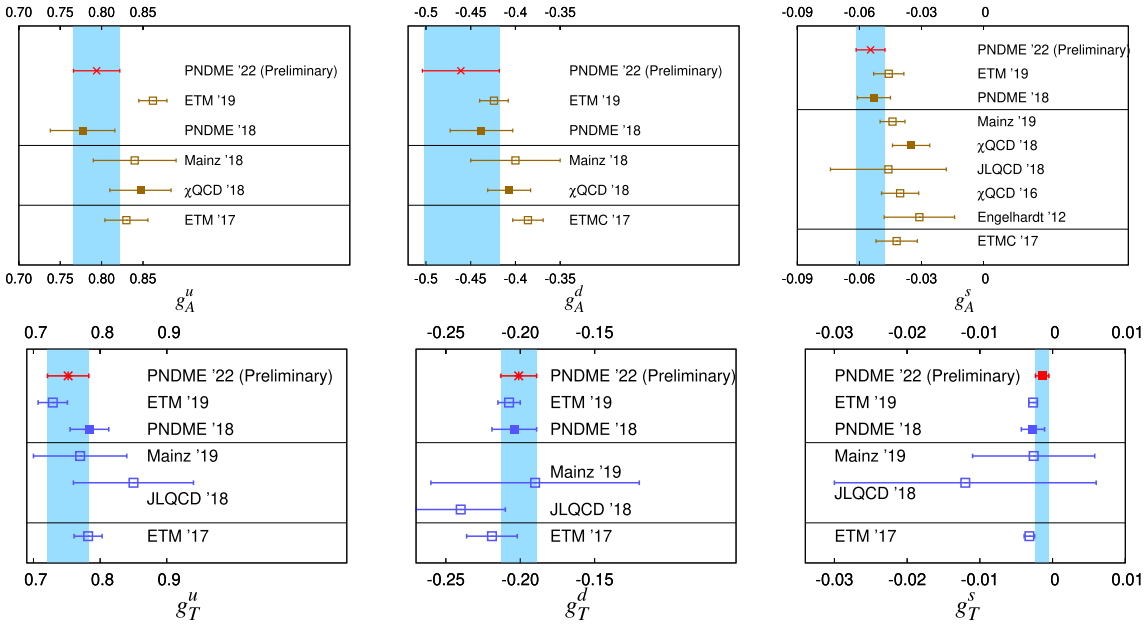

Fig. 2 Lattice results for g_A^q (top) and g_T^q (bottom) added to the FLAG 2021 summary figure [18] (references within). Figure taken from Ref. [17]

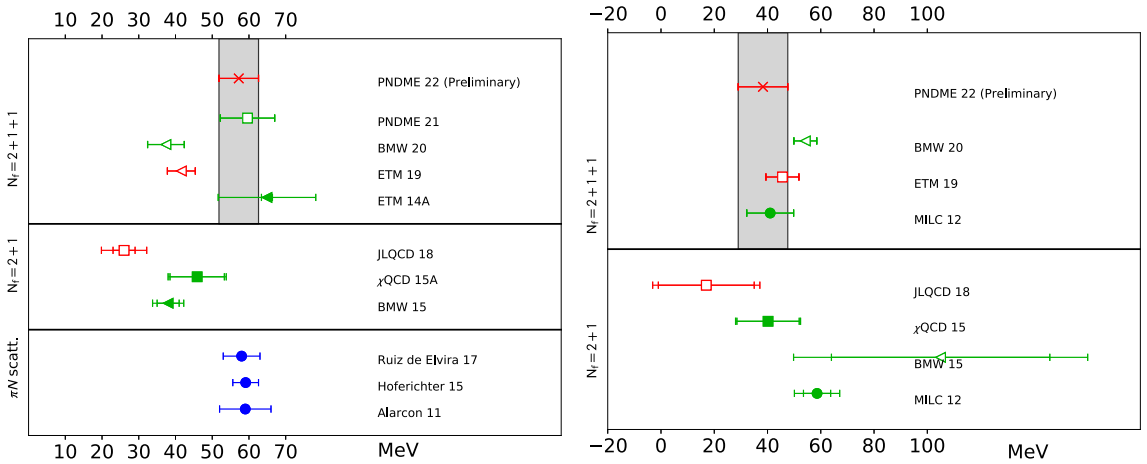

Fig. 3 Summary of the pion-nucleon sigma term and the strangeness content of the nucleon. For details and references to other lattice calculations, see Refs. [17–19]

around 0.4, where global fits prefer. Higher-precision lattice calculations are needed with order-of-magnitude increases in computational resources to reduce the errors to be comparable with those from global fits (using more than 60 years of experimental data).

Another example taken from PNDME collaboration on their recent update on the nucleon charges (Fig. 2) and σ term (Fig. 3), which also feature simultaneous chiral-continuum fits [17].

3 Bjorken-x-Dependent Hadron Structure

Since 2013, numerous calculations of x-dependent hadron structure in lattice QCD have emerged since the proposal of Large-Momentum Effective Theory (LaMET) [20–22]. Many lattice works have been done on nucleon and meson PDFs and GPDs based on the quasi-PDF approach [23–41,41–53,53,54,54–58]. Alternative approaches to access x-dependent structure in lattice QCD are also proliferating; for example, the Compton-amplitude approach (or "OPE without OPE") [59–71], the "hadronic-tensor approach" [72–77], the

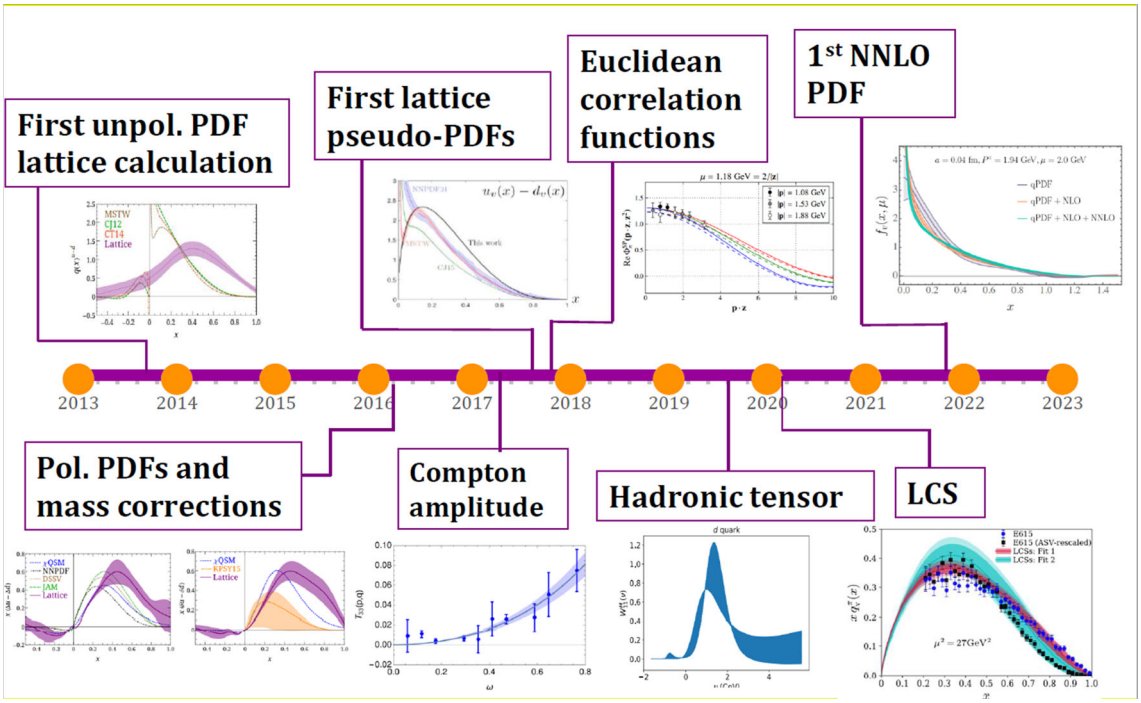

Fig. 4 A timeline showing the rapid development of the lattice methods for x-dependent hadron structure calculations, starting from the quasi-PDF (or LaMET method) in unpolarized and polarized isovector nucleon calculation, toward first of the many methods used in different approaches and hadron structure

"current-current correlator" [49,66,78–83] and the pseudo-PDF approach [81,84–103]. A few works have started to include lattice-QCD systematics, such as finite-volume effects [40,83] and lattice-spacing dependence for quark [45,50,52,104–106] and gluon [100,102,103] distributions, in their x-dependent structure calculations. Most lattice calculations of PDFs use next-to-leading-order (NLO) matching [22,107–109], but recently some lattice calculations of the valence pion PDF [110] have incorporated NNLO matching [47,111]. Figures 4 and 5 shows the important milestones that has been made in lattice QCD in x-dependent hadron structure in the past decade. We refer interested readers to these recent reviews for more details on lattice moments [1–3,112].

3.1 Recent Lattice PDF Progress

Isovector nucleon and the valence-quark pion PDFs are the most commonly calculated quantities on the lattice. Reference [1] has summarized a few selected significant results there, including post-2020 meson gluon PDF calculation. For the remaining of this subsection, we will show a few selected new development since the writeup of Ref. [1] and highlighted an impact study on the lattice x-dependent quantities toward PDFs.

3.1.1 Gluon PDFs

The gluon PDF $g(x)$ needs to be known precisely to calculate the cross section for these processes in pp collisions, such as the cross section for Higgs-boson production and jet production at the Large Hadron Collider (LHC) [113,114], and direct J/ψ photoproduction at Jefferson Lab [115]. A state-of-the-art lattice the nucleon gluon PDF was recently reported by MSULat group [103] at the physical pion mass and continuum limit. The continuum-physical RpITD band are shown on the left plot of Fig. 6 with all the data points from the four ensembles (with lattice spacing of 0.09, 0.12, and 0.15 fm) and a and a^2 extrapolation to the continuum-physical band. The open symbols indicate the strange-mass nucleon calculation from the ensemble. The unpolarized nucleon gluon PDF $xg(x)$ can be extracted by taking the ratio of $f_g(x,\mu) = xg(x,\mu)/\langle x\rangle_g(\mu)$ and the gluon momentum fraction $\langle x\rangle_g(\mu)$ obtained in Ref. [16]. The first physical-continuum limit unpolarized nucleon

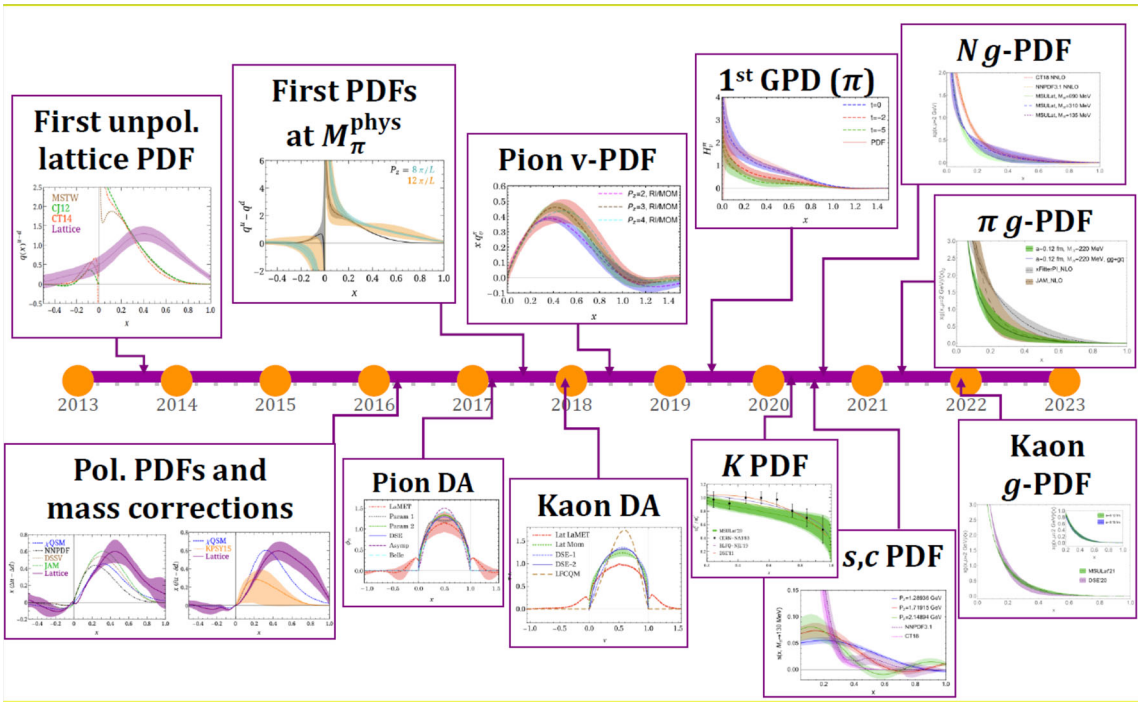

Fig. 5 Timeline from 2013 to 2023 of the first x-dependent observables calculated on the lattice

gluon PDF is shown as green bands in Fig. 6 which has reasonable agreement with the global fits from CT18 [9] and NNPDF3.1 [10] NNLO analysis for $x \in [0.25, 1]$. Tension with the gluon PDF from JAM20 [116] for $x < 0.6$ is observed, though its gluon PDF also behaves quite differently from the CT18 and NNPDF results, even with smaller errors. Future updates to the experimental data may help resolve this discrepancy in the global-fit community. All the lattice-QCD calculations of $xg(x)$ are also summarized: the cyan bands in Fig. 6 show the first pseudo-PDF calculation done using clover-on-HISQ with 0.12-fm lattice spacing and 310- and 700-MeV pion mass using 898 lattice configurations with 32 sources per configuration for the nucleon two-point correlators[96]. The results are extrapolated to physical pion mass using naive extrapolation of the two valence pion masses with $xg(x)$ reconstructed by multiplying the gluon momentum fraction taken from Ref. [56]. The blue bands in Fig. 6 show a followup calculation performed by HadStruc Collaboration using 2+1 dynamical flavors of clover fermions with stout-link smearing on the gauge fields, 0.09-fm lattice spacing, 358-MeV pion mass, and 64 source measurements on 349 lattice configurations with gradient-flow improved gluonic operators [99]. Multiple nucleon interpolating fields were used, allowing them to use generalized eigenvalue method to determine the best overlap with ground-state nucleon gluonic matrix elements. However, the gluon momentum fraction is taken from another lattice work, rather than directly calculated on the same lattice setup where the gluon PDF is calculated; this introduces some systematics at finite lattice spacing. MSULat's results on a single lattice-spacing ensemble (0.09 fm) are shown as a purple band in Fig. 6; this used about 300k measurements spread out over 1000 lattice configurations. Without the additional error propagation introduced by taking physical-continuum extrapolation, the single-ensemble results have errors comparable to (in some regions, smaller than) CT18 and NNPDF. The lattice-spacing and pion-mass here is similar to those used in the HadStruc calculation [99] but without the additional uncertainties due to continuum-physical extrapolation (shown as a green band). There are noticeable deviations from the HadStruc results, especially in the larger-x region; HadStruc's large-x gluon PDF is much smaller than MSULat's. However, given that multiple methodological aspects are done quite differently (for example, MSULat used the momentum fraction from the same lattice ensemble while HadStruc do not and use a different gluon-operator smearing), it may require the full calculation, including continuum-physical extrapolation, to meaningfully compare them. All the prior single-ensemble lattice results (without the systematics from lattice discretization) agree with the lattice continuum-physical $xg(x)$ due to the larger total errors from the continuum-physical extrapolation. Future work to include finer lattice-spacing and lighter pion masses in the extrapolation will help to improve the continuum-physical determination of the lattice gluon PDF.

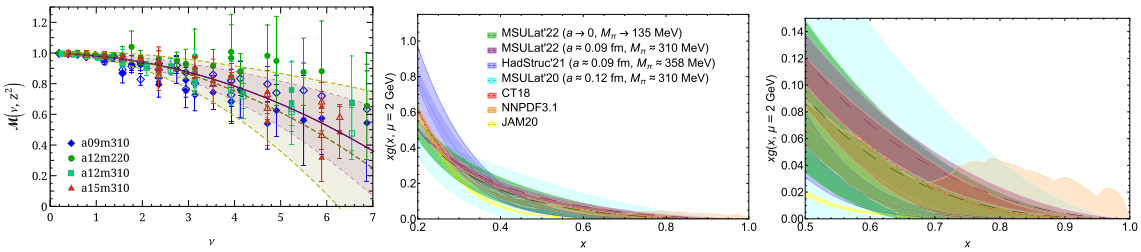

Fig. 6 (Left) Collected data for all ensembles with a (dashed band) and a^2 (solid band) continuum extrapolation at the physical pion mass. Open symbols indicates the data point from the same-symbol ensemble but at the heavier quark mass. The unpolarized gluon PDF, $xg(x, \mu)$ a function of x with $x \in [0.2, 1]$ (middle) region as and a close-look of the large-x region (right), obtained from our continuum-physical (green) and a09m310-ensemble (purple) RpITDs compared with a single-ensemble analysis from HadStruc ($a \approx 0.094$ fm, $M_\pi \approx 358$ MeV), and the CT18 NNLO [9] (red band), NNPDF3.1 NNLO [10] (orange ban) and JAM20 [116] (yellow band) gluon PDFs at $\mu = 2$ GeV in the $\overline{\text{MS}}$ scheme. Other lattice calculations of $xg(x)$ (including those done at single ensemble) from HadStruc [99] (blue band) and MSULat [96] (cyan band) are also shown in the plot. The lattice PDF results are consistent with the CT18 NNLO and NNPDF3.1 NNLO unpolarized gluon PDFs within errors. Plots taken from Ref. [103]

3.1.2 Strange PDF and Impacts on Global PDFs

Lattice calculation can determine the strangeness asymmetry $s_-(x) \equiv s(x) - \bar{s}(x)$, removing one of the assumptions used in the global fit and thereby reducing global-fit errors. Since strangeness asymmetry is flavor-singlet, we can confidently calculate it using LaMET coordinate-space matrix elements on the lattice. However, since the "disconnected" quark diagram is needed for the strangeness matrix elements, the computational cost is very expansive, and there have only been a handful of lattice calculations. In the work of Ref. [117], the lattice matrix elements are computed on a single 0.12-fm lattice ensemble using two valence masses for the nucleon: light ($M_\pi \approx 310$ MeV) and strange ($M_\pi \approx 690$ MeV). The left-hand side of Fig. 7 shows the lattice real matrix elements at $M_\pi = 135$ MeV (extrapolated linearly in M_π^2) with nucleon boost momenta $P_z \in [1.3, 2.2]$ compared with the CT18 NNLO (red band with dot-dashed line) and NNPDF3.1 NNLO (orange band with dotted line) gluon PDFs. The real matrix elements are proportional to the integral of the difference between strange and antistrange PDFs ($\int dx\,(s(x) - \bar{s}(x))\cos(xzP_z)$), where z is the Wilson-line displacement as shown in Fig. 3 of Ref. [46]. The lattice results of the real quasi-PDF matrix elements, as shown in Fig. 7, are consistent with zero at 95% confidence level for most zP_z points, indicating that the strange quark-antiquark asymmetry is likely very small.

To take advantage of existing lattice data to reach a wider region of x, Ref. [117] choose to focus on the result of $P_z \approx 1.7$ GeV. The renormalized matrix elements were Fourier transformed into quasi-PDFs by using the extrapolation formulation suggested in Ref. [118] to fit the large-$|z|$ data to the formula $c_1(-izP_z)^{-d_1} + c_2 e^{izP_z}(izP_z)^{-d_2}$, inspired by the Regge behavior. Extrapolating the matrix elements into the region beyond the lattice calculation then suppresses Fourier-transformation artifacts. The quasi-PDF can be related to the P_z-independent lightcone PDF at scale μ in $\overline{\text{MS}}$ scheme through a factorization theorem [21]. The quasi- and matched strangeness asymmetry distributions as functions of x can be found on the right-hand side of Fig. 7; both are consistent with zero. Note that the matching from quasi-PDF to PDF has residual systematics at $O\left(\frac{\Lambda^2_{\text{QCD}}}{(xP_z)^2}\right)$ and $O\left(\frac{\Lambda^2_{\text{QCD}}}{(1-x)^2P_z^2}\right)$ at very small x and x near 1, respectively. From the isovector nucleon PDF study, at this P_z boost momentum, we can reasonably rely on lattice x-dependent strange asymmetry for $x \in [0.3, 0.8]$ with interval of 0.01 jackknife sampling. Beyond this region, the lattice errors could increase significantly due to the systematics at finite momentum.

The lattice data for the strangeness asymmetry is then taken as a constraint to the global PDF fit to obtain a new distribution, CT18As_Lat PDFs, using Lagrange-multiplier method [119]. The uncertainty of lattice calculation is treated as the uncorrelated error during the fitting with quality-of-fit

$$\chi^2 = \chi^2_{\text{Exp.}} + \sum_i \left(\frac{s_v^{\text{para.}}(x_i) - s_v^{\text{Lat.}}(x_i)}{\Delta s_v^{\text{Lat.}}(x_i)}\right)^2, \tag{2}$$

where $\chi^2_{\text{Exp.}}$ is the total χ^2 for fitting experimental data. Table 1 shows the changes with and without lattice data.

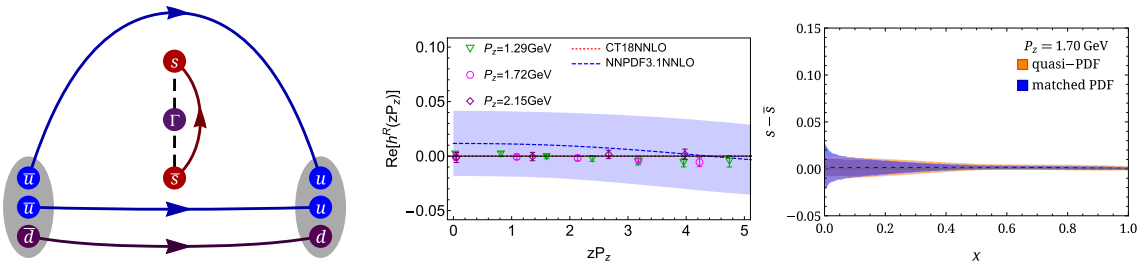

Fig. 7 (left) Illustration of the three-point correlation function involving a strange-quark long-link operator, which forms a disconnected diagram. The dashed line indicates the spatial displacement of the Wilson link with the choice of operator Γ. The gray blobs show the nucleon source and sink, separated by $t_{\rm sep}$ in Euclidean time direction. Sea-quark and gluon interactions, although present in the lattice configurations, are omitted from this schematic diagram. (middle) The real parts of the strange quasi-PDF matrix elements in coordinate space from our calculations at physical pion mass with $P_z \in [1.3, 2.15]$ GeV [46], along with those from CT18 and NNPDF NNLO. (right) The quasi (orange) and matched (blue) valence strange distribution from LQCD calculation

Table 1 The total goodness-of-fit $\chi^2_{\rm tot}$ of the CT18A, CT18As, and CT18As_Lat fits, respectively, at $Q_0 = 1.3$ GeV. The total number of data points (without including the lattice data) of each fit is 3674

PDF	$s_-(x, Q_0)$	Lat. data	$\chi^2_{\rm tot}$
CT18A	0	No	4376
CT18As	$\neq 0$	No	4344
CT18As_Lat	$\neq 0$	Yes	4361

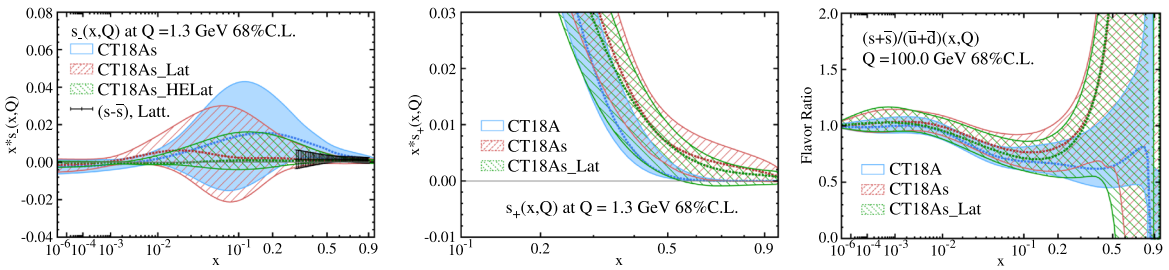

Fig. 8 The comparison of $s_-(x)$ (left), $s_+(x)$ (middle) PDFs at the initial Q_0 scale, as well as $(s + \bar{s})/(s - \bar{s})(x)$ (right) at $Q = 100$ GeV, for CT18A, CT18As, and CT18As_Lat. Note that in the middle-left panel, predictions of the strangeness asymmetry of CT18A and CT18As_Lat are compared to the current lattice data and expected improvement if current lattice data errors are reduced by a half (green backslashed area, i.e., CT18As_HELat). For CT18A, no strangeness asymmetry $s_-(x)$ is allowed at the initial Q_0 scale in the nonperturbative parametrization, so CT18A is absent in the comparison plot of $s_-(x)$. Plots taken from Ref. [117]

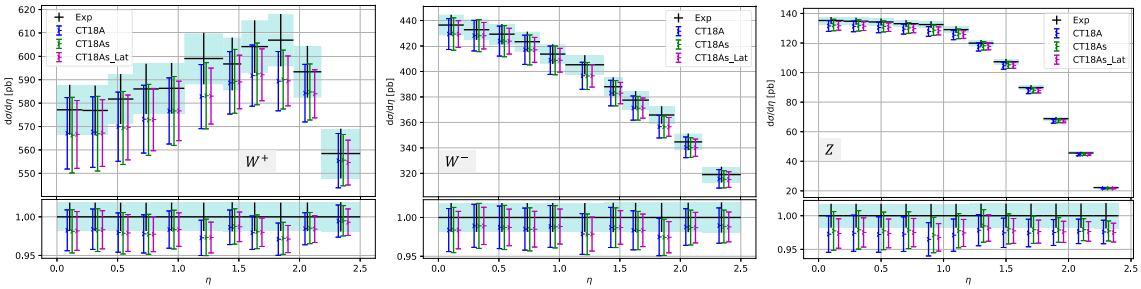

Fig. 9 Comparison of CT18A, CT18As, and CT18As_Lat predictions to the experimental values of ID=248 ATLAS 7-TeV W and Z differential cross sections for W^+ (left), W^- (middle), Z (right) as functions of dilepton pseudorapidity [120]. Plots taken from Ref. [117]

The leftmost part of Fig. 8 shows the impact of lattice data on the strangeness asymmetry $s_-(x)$. The lattice data points are distributed in the region of $0.8 \geq x \geq 0.3$, and they are consistent with a very small strangeness asymmetry with high precision. Compared to the error band of CT18As, the uncertainty in lattice data points is quite small, so that including the lattice data in the CT18As_Lat fit greatly reduces the size of the s_--PDF error band in the large-x region. The amount of reduction of the CT18As_Lat error band in the much smaller x region is likely to depend on the chosen nonperturbative parametrization form of $s_-(x)$ at $Q_0 = 1.3$ GeV. Hence, it is important to have more precise lattice data, extended to smaller x values. Based on the CT18As_Lat PDF, it is further investigated how much the lattice data with higher precision would be able to constrain the s_- distribution. By reducing the uncertainty of lattice data points by half, one results in another PDF labelled “CT18As_HELat" and this shows even strong power in further constraining s_-, reducing the error band of s_- by nearly a factor of two in the large-x region. The comparison of the total strangeness $s_+(x)$ at $Q_0 = 1.3$ GeV is shown in middle of Fig. 8. In CT18As, the central value of the total strangeness $s_+(x)$ is enhanced across a wide range of x relative to CT18A. The uncertainty of s_+ in CT18As is also enlarged. The similar behaviour can also be observed in the ratios of strange asymmetry to total strangeness $s_-/\,s_+$ and total strangeness to light quarks $(s+\bar{s})/(\bar{u}+\bar{d})(x)$ at $Q = 100$ GeV, as shown in the rightmost panel of Fig. 8. Despite of the large uncertainty of the PDF ratio $(s+\bar{s})/(\bar{u}+\bar{d})(x)$ in the large-x region, the enhancement of $(s+\bar{s})/(\bar{u}+\bar{d})(x)$ in CT18As suggests a greater total strangeness than light-quark content. This feature is caused by the choice of the more flexible non-perturbative parametrization form of the (anti)strange PDF adopted in the CT18As fit, as compared to that in CT18.

The phenomenological impact of ATLAS 7-TeV W and Z production data from the LHC was also investigated in Ref. [117]. The ATLAS 7-TeV W and Z data are compared to the theoretical predictions of CT18A, CT18As, and CT18As_Lat in Fig. 9. The central values of the predictions for all the W and Z data are below the experimental measurements and on the edge or even outside of the experimental error bands. However, considering PDF-induced uncertainties, all predictions are consistent with the experimental measurements. The differences among the predictions of CT18A, CT18As, and CT18As_Lat for $W^{\pm}$ production (the right and middle plots of Fig. 9) are small, compared to the large uncertainty. It is noted that in Ref. [117], by allowing a nonvanishing strangeness asymmetry at Q_0 scale, the reduced χ^2 for the W^- production data is improved, while it is almost unchanged for the W^+ production data. The improvement relative to the W^- production (via $s\bar{u}, s\bar{c} \to W^-$) data can be understood from Fig. 8, where $s(x)$ is enhanced with a nonvanishing strangeness asymmetry, while $\bar{s}(x)$ is less affected. In CT PDF global analysis [119,121], the χ^2 of a certain experimental measurement receives contributions from two parts, $\chi^2 = \chi^2_{\text{red.}} + R^2$. The term R^2 is the sum of the squares of nuisance parameters associated with each of the correlated systematic uncertainties, and it is analytically minimized with respect to the current optimal PDF. The other part, referred as the reduced chi-square $\chi^2_{\text{red.}}$, quantifies the difference between theory prediction and shifted data, in units of the total uncorrelated uncertainty, including both statistical and uncorrelated systematic errors, of every data point. As for the Z-boson–production (the right-hand side of Fig. 9), the CT18As prediction is slightly larger than CT18A. Since the production of Z-bosons via the Drell-Yan process is dominated by quark-antiquark fusion, the enhancement in the Z production rate reflects a higher magnitude in the combination of quark and antiquark PDFs. This can be seen in Fig. 8, which shows the total strangeness $s_+(x)$ receiving a higher magnitude if nonzero strangeness asymmetry $s_-(x)$ is allowed. Relative to CT18As, the CT18As_Lat prediction is shifted such that it becomes closer to that of CT18A. Meanwhile, the predicted uncertainty of CT18As_Lat shrinks compared to CT18As.

3.2 Applications to Generalized Parton Distributions

Generalized parton distributions provide hybrid momentum and coordinate space distributions of partons and bridge the standard nucleon structure observables: form factors and collinear PDFs. More importantly, GPDs provide information on the spin and mass structure of the nucleon. GPDs bring the energy-momentum tensor matrix elements within experimental grasp through electromagnetic scattering and can be viewed as a hybrid of parton distributions (PDFs), form factors, and distribution amplitudes. For example, the forward limit of the unpolarized and helicity GPDs lead to the $f_1(x)$ and $g_1(x)$ PDFs, respectively. Taking the integral over x at finite values of the momentum transfer results in the form factors and generalized form factors. In the case of the unpolarized GPDs, for example, one obtains the Dirac (F_1) and Pauli (F_2) form factors. Several of these limits of the GPDs have physical interpretations, for instance, the spin decomposition of the proton using Ji's sum rule [122].

Information on GPDs from lattice QCD has been available via their form factors and generalized form factors, using the operator product expansion (OPE). As in PDFs, such information is limited due to the suppression of the signal as the order of the Mellin moments increases and the momentum transfer between the initial and final state increases. Significant progress has been made towards new methods to access the x- and t-dependence of GPDs ($t = -Q^2$), which is driven by the advances in PDF calculations. In lattice QCD, there are several challenges in calculating GPD using these new methods. The extraction of GPDs is more challenging than collinear PDFs, because GPDs require momentum transfer, Q^2, between the initial (source) and final (sink) states. Another complication is that GPDs are defined in the Breit frame, in which the momentum transfer is equally distributed to the initial and final states; such a setup increases the computational cost, as separate calculations are necessary for each value of the momentum transfer.

The first lattice x-dependent GPD calculations were carried out in Ref. [41], studying the pion valence-quark GPD at zero skewness with multiple transfer momenta with pion mass $M_\pi \approx 310$ MeV. There is a reasonable agreement with traditional local-current form-factor calculations at similar pion mass, but the current uncertainties remain too large to show a clear preference among different model assumptions about the kinematic dependence of the GPD. There has also been recent progress made in lattice QCD to provide the Bjorken-x dependence of the isovector nucleon GPDs, H, E and $\tilde{H}$. Ref. [53] used LaMET to calculate both unpolarized and polarized nucleon isovector GPDs with largest boost momentum 1.67 GeV at pion mass $M_\pi \approx 260$ MeV with one momentum transfer. This work also presented results at nonzero skewness, with additional divergence near $x = \xi$ due to the matching. Refs. [54,57] reported the first lattice-QCD calculations of the unpolarized and helicity nucleon GPDs with boost momentum around 2.0 GeV at physical pion mass with multiple transfer momenta, allowing study of the three-dimensional structure and impact-parameter–space distribution. Results for the moments of the integral of the H, E and $\tilde{H}$ GPDs extracted from the lattice are within a couple sigma of previous lattice calculations using OPE operators from traditional form factors and generalized form factors at or near the physical pion mass. Such lattice inputs can provide useful constraints to the best determination of physical quantities using both theoretical and experimental inputs. These results have been included in Ref. [1]. Progress so far has been done using Breit frame, where the initial and final momenta of the hadron differ by half the transfer momentum. Recent work on asymmetric momentum setups for GPDs has been demonstrated by ETM and BNL/ANL groups [58].

For the pion GPD, there is an ongoing lattice-QCD x-dependent pion valence-quark GPD by MSULat group calculated directly at physical pion mass using the LaMET with next-to-next-to-leading order perturbative matching correction; the pion two-point measurements number up to $O(10^6)$ with boost momentum 1.73 GeV. The pion valence distribution is renormalized in hybrid scheme with Wilson-line mass subtraction at large distances in coordinate space, followed by a procedure to match it to the $\overline{MS}$ scheme. The results are shown in Fig. 10. The pion form factors obtained from taking the moments of the pion GPD function, with two recent lattice calculations using vector current operator, are summarized In the right-most plot of Fig. 10. χQCD Collaboration used overlap fermions on seven ensembles of 2+1-flavor domain-wall configurations, including multiple lattice spacings $a \in [0.083, 0.195]$ fm to remove lattice discretization effects, and pion masses ranging from 139 to 340 MeV. Their statistics range from 9,600 to 485,376 measurements [123]. BNL used clover on $N_f = 2 + 1$ HISQ lattice at a single lattice spacing $a = 0.076$ fm at physical pion mass with 35,000 measurements (with two additional ensembles at smaller lattice-spacing with 300-MeV pion to quantify the systematics) [124]. We can see that there is a very nice agreement among all the lattice results, even through the lattice spacing varies among the three calculations. The lattice pion form factors are also compared with those extracted from experiments [125–129] and find good agreement; the lattice data are more precise than the available experimental data in certain transfer-momentum regions.

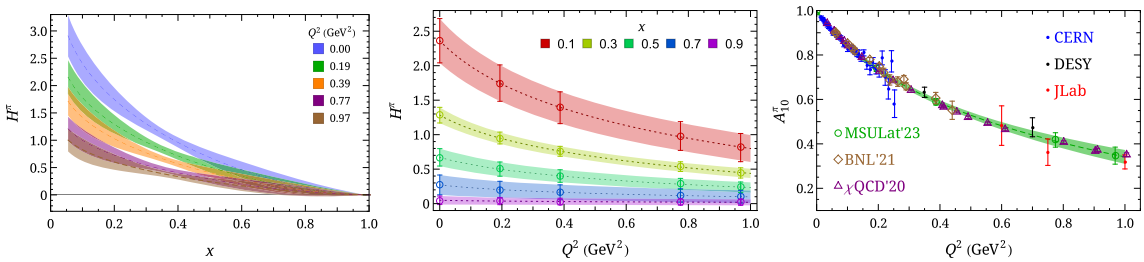

Fig. 10 (Left) Pion valence-quark GPD as a function of Bjorken-x with five values of transfer momenta. (Middle) Pion valence-quark GPD as a function of transfer momenta with selected Bjorken-x indicated in the bands. The z-expansion is used to extrapolated the five points of transfer momenta. (Right) Selected pion form factor $F_\pi(Q^2)$ at the physical pion mass flavours of light quarks from different lattice groups (labeled "χQCD'20" [123], "BNL'21" [124]), together with the result obtained in this work (labeled "MSULat'23") and experimental data [130]. We found that this leading moments of our pion GPD is in agreement with prior lattice works and existing experimental data [125–129]

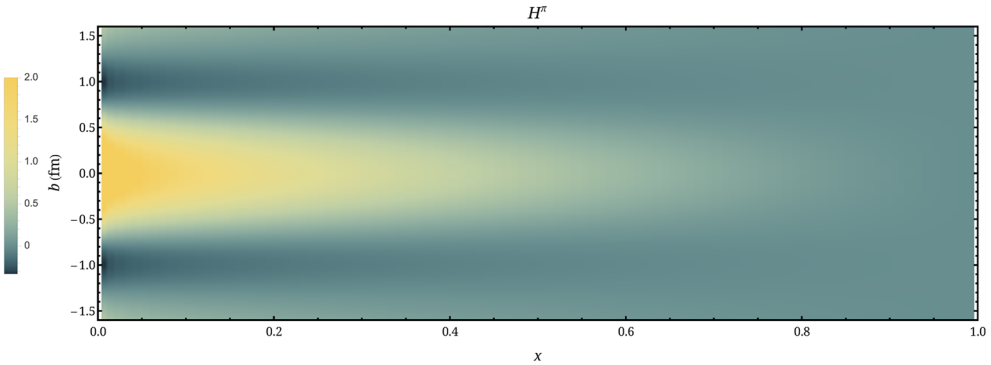

Fig. 11 The valence-quark impact-parameter–dependent distribution of pion as a function of b and x

Taking the lattice calculations of the pion valence-quark GPD, $H_\pi(x, \xi = 0, Q^2)$, we can then Fourier transform of this GPD to learn about the impact-parameter–dependent distribution, $\mathsf{q}(x, b)$ [131,132]: $\mathsf{q}^\pi(x, b) = \int \frac{d\mathbf{q}}{(2\pi)^2} H^\pi(x, \xi = 0, t = -\mathbf{q}^2) e^{i\mathbf{q}\cdot\mathbf{b}}$, where b is the light-front distance from the center of transverse momentum (CoTM). Figure 11 shows the slices of the such distribution with selected $x \in [0.1, 0.9]$, as well as two-dimensional distributions at $x = 0.45$. The impact-parameter–dependent distribution describes the probability density for a parton with momentum fraction x to be found in the transverse plane at distance b from the CoTM. It provides a snapshot of the pion in the transverse plane and indicates what might be expected from pion tomography.

3.3 Future Prospects and Challenges

Computing lattice matrix elements suitable for parton physics faces a number of challenges beyond the broad requirements of most lattice calculations for small lattice spacing, large volume, and physical pion mass. First and foremost is the large momentum necessary in hadron states (P_μ). The second, relevant to Wilson-line operators, is renormalization of Wilson-line operators that have linear divergences requiring high-precision control of UV physics. The third is the long-range correlations in coordinate space necessary for small and large x partons and for TMD impact-parameter space calculations in LaMET. Fourth, some approaches in extracting x-dependent PDFs require solving in inverse problem which is a challenge on controllable systematics. Finally, in calculations involving large P_z and z, gluonic observables, and quantities depending on multi-variables such as GPDs, poor signal-to-noise ratios ensure that significant computational resources are required, and thus new methods that can accelerate the standard calculations need to be systematically developed. We refers interested readers to the 2022 Snowmass whitepaper [112] for more discussion on these topics and references within.

4 Conclusion and Outlook

In the past decade, there have been tremendous breakthroughs in LQCD that enable us to compute from first principles the emergent quark and gluon structures inside nucleons and nuclei. These advances are opening new venues to access parton degrees of freedom encoded in quantities such as PDFs and GPDs. In principle, such calculations have the potential to enable ab-initio predictions for hard processes in higher-energy reactions that can be compared directly with experimental data and provide a better understanding of QCD's emergent phenomena, as well as more reliable Standard-Model inputs to aid new-physics searches in many nuclear physics and high-energy physics frontiers.

However, currently, the precision of LQCD calculations are highly limited by the availability of computational resources and more are needed to achieve the ideal ab-initio predictions that can be tested experimentally. In this review, we have summarized the state of the art for selected example calculations and the associated computational challenges. We have also discussed the potential complementary and synergistic combinations with QCD global analysis using current precision LQCD calculations. Polarized structure from LQCD calculations are competitive with experimental data and allows us to carryout a *hybrid* QCD global analysis, combining lattice and experimental data within a suitable Bayesian inference framework. In the unpolarized case, there has been first work showing that strange quark distribution from lattice calculation can have important impact and further reducing lattice error can significantly enhance our understands on hadron structure. Similar synergies can be also found in the context of meson structures relevant for future programs at AMBER at CERN and the tagged experiments at Jefferson Lab and the future EIC. Moreover, for GPD studies, it is expected that Lattice-QCD inputs will become increasingly important to support programs for three-dimensional imaging of nucleons and nuclei at Jefferson Lab and the future EIC. With sufficient computational support, Lattice-QCD calculations can reach precision comparable with experimental data, which will greatly benefit the nuclear physics and high-energy physics communities.

Acknowledgements This work of HL is partly supported by the NSF under grant PHY 2209424 & 1653405 and the Research Corpora on for Science Advancement through the Cottrell Scholar Award.

Declarations

Conflict of interest The authors declare no competing interests.

References

1. H.W. Lin, Few Body Syst. **63**(4), 65 (2022). https://doi.org/10.1007/s00601-022-01764-y
2. H.W. Lin et al., Prog. Part. Nucl. Phys. **100**, 107 (2018). https://doi.org/10.1016/j.ppnp.2018.01.007
3. M. Constantinou et al., Prog. Part. Nucl. Phys. **121**, 103908 (2021). https://doi.org/10.1016/j.ppnp.2021.103908
4. C. Alexandrou, S. Bacchio, M. Constantinou, J. Finkenrath, K. Hadjiyiannakou, K. Jansen, G. Koutsou, H. Panagopoulos, G. Spanoudes, Phys. Rev. D **101**(9), 094513 (2020). https://doi.org/10.1103/PhysRevD.101.094513
5. Y.B. Yang, M. Gong, J. Liang, H.W. Lin, K.F. Liu, D. Pefkou, P. Shanahan, Phys. Rev. D **98**(7), 074506 (2018). https://doi.org/10.1103/PhysRevD.98.074506
6. Y.B. Yang, J. Liang, Y.J. Bi, Y. Chen, T. Draper, K.F. Liu, Z. Liu, Phys. Rev. Lett. **121**(21), 212001 (2018). https://doi.org/10.1103/PhysRevLett.121.212001
7. C. Alexandrou, M. Constantinou, K. Hadjiyiannakou, K. Jansen, C. Kallidonis, G. Koutsou, A. Vaquero Avilés-Casco, C. Wiese, Phys. Rev. Lett. **119**(14), 142002 (2017). https://doi.org/10.1103/PhysRevLett.119.142002
8. N. Sato, C. Andres, J.J. Ethier, W. Melnitchouk, Phys. Rev. D **101**(7), 074020 (2020). https://doi.org/10.1103/PhysRevD.101.074020
9. T.J. Hou et al., Phys. Rev. D **103**(1), 014013 (2021). https://doi.org/10.1103/PhysRevD.103.014013
10. R.D. Ball et al., Eur. Phys. J. C **77**(10), 663 (2017). https://doi.org/10.1140/epjc/s10052-017-5199-5
11. S. Dulat, T.J. Hou, J. Gao, M. Guzzi, J. Huston, P. Nadolsky, J. Pumplin, C. Schmidt, D. Stump, C.P. Yuan, Phys. Rev. D **93**(3), 033006 (2016). https://doi.org/10.1103/PhysRevD.93.033006
12. L.A. Harland-Lang, A.D. Martin, P. Motylinski, R.S. Thorne, Eur. Phys. J. C **75**(5), 204 (2015). https://doi.org/10.1140/epjc/s10052-015-3397-6
13. S. Alekhin, J. Blümlein, S. Moch, R. Placakyte, Phys. Rev. D **96**(1), 014011 (2017). https://doi.org/10.1103/PhysRevD.96.014011
14. A. Accardi, L.T. Brady, W. Melnitchouk, J.F. Owens, N. Sato, Phys. Rev. D **93**(11), 114017 (2016). https://doi.org/10.1103/PhysRevD.93.114017
15. H. Abramowicz et al., Eur. Phys. J. C **75**(12), 580 (2015). https://doi.org/10.1140/epjc/s10052-015-3710-4
16. Z. Fan, H.W. Lin, M. Zeilbeck, Phys. Rev. D **107**(3), 034505 (2023). https://doi.org/10.1103/PhysRevD.107.034505

17. S. Park, T. Bhattacharya, R. Gupta, H.W. Lin, S. Mondal, B. Yoon, PoS Lattice **LATTICE2022**, 118 (2023). https://doi.org/10.22323/1.430.0118
18. Y. Aoki et al., Eur. Phys. J. C **82**(10), 869 (2022). https://doi.org/10.1140/epjc/s10052-022-10536-1
19. R. Gupta, S. Park, M. Hoferichter, E. Mereghetti, B. Yoon, T. Bhattacharya, Phys. Rev. Lett. **127**(24), 242002 (2021). https://doi.org/10.1103/PhysRevLett.127.242002
20. X. Ji, Phys. Rev. Lett. **110**, 262002 (2013). https://doi.org/10.1103/PhysRevLett.110.262002
21. X. Ji, Sci. China Phys. Mech. Astron. **57**, 1407 (2014). https://doi.org/10.1007/s11433-014-5492-3
22. X. Ji, J.H. Zhang, Y. Zhao, Nucl. Phys. B **924**, 366 (2017). https://doi.org/10.1016/j.nuclphysb.2017.09.001
23. H.W. Lin, PoS **LATTICE2013**, 293 (2014). https://doi.org/10.22323/1.187.0293
24. H.W. Lin, J.W. Chen, S.D. Cohen, X. Ji, Phys. Rev. D **91**, 054510 (2015). https://doi.org/10.1103/PhysRevD.91.054510
25. J.W. Chen, S.D. Cohen, X. Ji, H.W. Lin, J.H. Zhang, Nucl. Phys. B **911**, 246 (2016). https://doi.org/10.1016/j.nuclphysb.2016.07.033
26. H.W. Lin, J.W. Chen, T. Ishikawa, J.H. Zhang, Phys. Rev. D **98**(5), 054504 (2018). https://doi.org/10.1103/PhysRevD.98.054504
27. C. Alexandrou, K. Cichy, V. Drach, E. Garcia-Ramos, K. Hadjiyiannakou, K. Jansen, F. Steffens, C. Wiese, Phys. Rev. D **92**, 014502 (2015). https://doi.org/10.1103/PhysRevD.92.014502
28. C. Alexandrou, K. Cichy, M. Constantinou, K. Hadjiyiannakou, K. Jansen, F. Steffens, C. Wiese, Phys. Rev. D **96**(1), 014513 (2017). https://doi.org/10.1103/PhysRevD.96.014513
29. C. Alexandrou, K. Cichy, M. Constantinou, K. Hadjiyiannakou, K. Jansen, H. Panagopoulos, F. Steffens, Nucl. Phys. B **923**, 394 (2017). https://doi.org/10.1016/j.nuclphysb.2017.08.012
30. J.W. Chen, T. Ishikawa, L. Jin, H.W. Lin, Y.B. Yang, J.H. Zhang, Y. Zhao, Phys. Rev. D **97**(1), 014505 (2018). https://doi.org/10.1103/PhysRevD.97.014505
31. J.H. Zhang, X. Ji, A. Schäfer, W. Wang, S. Zhao, Phys. Rev. Lett. **122**(14), 142001 (2019). https://doi.org/10.1103/PhysRevLett.122.142001
32. C. Alexandrou, K. Cichy, M. Constantinou, K. Jansen, A. Scapellato, F. Steffens, Phys. Rev. Lett. **121**(11), 112001 (2018). https://doi.org/10.1103/PhysRevLett.121.112001
33. J.W. Chen, L. Jin, H.W. Lin, Y.S. Liu, Y.B. Yang, J.H. Zhang, Y. Zhao (2018)
34. J.H. Zhang, J.W. Chen, L. Jin, H.W. Lin, A. Schäfer, Y. Zhao, Phys. Rev. D **100**(3), 034505 (2019). https://doi.org/10.1103/PhysRevD.100.034505
35. C. Alexandrou, K. Cichy, M. Constantinou, K. Jansen, A. Scapellato, F. Steffens, Phys. Rev. D **98**(9), 091503 (2018). https://doi.org/10.1103/PhysRevD.98.091503
36. H.W. Lin, J.W. Chen, X. Ji, L. Jin, R. Li, Y.S. Liu, Y.B. Yang, J.H. Zhang, Y. Zhao, Phys. Rev. Lett. **121**(24), 242003 (2018). https://doi.org/10.1103/PhysRevLett.121.242003
37. Z.Y. Fan, Y.B. Yang, A. Anthony, H.W. Lin, K.F. Liu, Phys. Rev. Lett. **121**(24), 242001 (2018). https://doi.org/10.1103/PhysRevLett.121.242001
38. Y.S. Liu, J.W. Chen, L. Jin, R. Li, H.W. Lin, Y.B. Yang, J.H. Zhang, Y. Zhao (2018)
39. W. Wang, J.H. Zhang, S. Zhao, R. Zhu, Phys. Rev. D **100**(7), 074509 (2019). https://doi.org/10.1103/PhysRevD.100.074509
40. H.W. Lin, R. Zhang, Phys. Rev. D **100**(7), 074502 (2019). https://doi.org/10.1103/PhysRevD.100.074502
41. J.W. Chen, H.W. Lin, J.H. Zhang, Nucl. Phys. B **952**, 114940 (2020). https://doi.org/10.1016/j.nuclphysb.2020.114940
42. H. Liu, Int. J. Mod. Phys. A **35**(11n12), 2030006 (2020). https://doi.org/10.1142/S0217751X20300069
43. Y. Chai et al., Phys. Rev. D **102**(1), 014508 (2020). https://doi.org/10.1103/PhysRevD.102.014508
44. S. Bhattacharya, K. Cichy, M. Constantinou, A. Metz, A. Scapellato, F. Steffens, Phys. Rev. D **102**(11), 111501 (2020). https://doi.org/10.1103/PhysRevD.102.111501
45. H.W. Lin, J.W. Chen, Z. Fan, J.H. Zhang, R. Zhang, Phys. Rev. D **103**(1), 014516 (2021). https://doi.org/10.1103/PhysRevD.103.014516
46. R. Zhang, H.W. Lin, B. Yoon, Phys. Rev. D **104**(9), 094511 (2021). https://doi.org/10.1103/PhysRevD.104.094511
47. Z.Y. Li, Y.Q. Ma, J.W. Qiu, Phys. Rev. Lett. **126**(7), 072001 (2021). https://doi.org/10.1103/PhysRevLett.126.072001
48. Z. Fan, X. Gao, R. Li, H.W. Lin, N. Karthik, S. Mukherjee, P. Petreczky, S. Syritsyn, Y.B. Yang, R. Zhang, Phys. Rev. D **102**(7), 074504 (2020). https://doi.org/10.1103/PhysRevD.102.074504
49. X. Gao, L. Jin, C. Kallidonis, N. Karthik, S. Mukherjee, P. Petreczky, C. Shugert, S. Syritsyn, Y. Zhao, Phys. Rev. D **102**(9), 094513 (2020). https://doi.org/10.1103/PhysRevD.102.094513
50. H.W. Lin, J.W. Chen, R. Zhang (2020)
51. K. Zhang, Y.Y. Li, Y.K. Huo, A. Schäfer, P. Sun, Y.B. Yang, Phys. Rev. D **104**(7), 074501 (2021). https://doi.org/10.1103/PhysRevD.104.074501
52. C. Alexandrou, K. Cichy, M. Constantinou, J.R. Green, K. Hadjiyiannakou, K. Jansen, F. Manigrasso, A. Scapellato, F. Steffens, Phys. Rev. D **103**, 094512 (2021). https://doi.org/10.1103/PhysRevD.103.094512
53. C. Alexandrou, K. Cichy, M. Constantinou, K. Hadjiyiannakou, K. Jansen, A. Scapellato, F. Steffens, Phys. Rev. Lett. **125**(26), 262001 (2020). https://doi.org/10.1103/PhysRevLett.125.262001
54. H.W. Lin, Phys. Rev. Lett. **127**(18), 182001 (2021). https://doi.org/10.1103/PhysRevLett.127.182001
55. X. Gao, K. Lee, S. Mukherjee, C. Shugert, Y. Zhao, Phys. Rev. D **103**(9), 094504 (2021). https://doi.org/10.1103/PhysRevD.103.094504
56. M. Constantinou et al., Prog. Part. Nucl. Phys. **121**, 103908 (2021). https://doi.org/10.1016/j.ppnp.2021.103908
57. H.W. Lin, Phys. Lett. B **824**, 136821 (2022). https://doi.org/10.1016/j.physletb.2021.136821
58. S. Bhattacharya, K. Cichy, M. Constantinou, J. Dodson, X. Gao, A. Metz, S. Mukherjee, A. Scapellato, F. Steffens, Y. Zhao, Phys. Rev. D **106**(11), 114512 (2022). https://doi.org/10.1103/PhysRevD.106.114512
59. U. Aglietti, M. Ciuchini, G. Corbo, E. Franco, G. Martinelli, L. Silvestrini, Phys. Lett. B **441**, 371 (1998). https://doi.org/10.1016/S0370-2693(98)01138-1
60. G. Martinelli, Nucl. Phys. B, Proc. Suppl. **73**, 58 (1999). https://doi.org/10.1016/S0920-5632(99)85007-5

61. C. Dawson, G. Martinelli, G.C. Rossi, C.T. Sachrajda, S.R. Sharpe, M. Talevi, M. Testa, Nucl. Phys. B **514**, 313 (1998). https://doi.org/10.1016/S0550-3213(97)00756-6
62. S. Capitani, M. Gockeler, R. Horsley, H. Oelrich, D. Petters, P.E.L. Rakow, G. Schierholz, Nucl. Phys. B, Proc. Suppl. **73**, 288 (1999). https://doi.org/10.1016/S0920-5632(99)85050-6
63. S. Capitani, M. Gockeler, R. Horsley, D. Petters, D. Pleiter, P.E.L. Rakow, G. Schierholz, Nucl. Phys. B, Proc. Suppl. **79**, 173 (1999). https://doi.org/10.1016/S0920-5632(99)00666-0
64. X.D. Ji, C.W. Jung, Phys. Rev. Lett. **86**, 208 (2001). https://doi.org/10.1103/PhysRevLett.86.208
65. W. Detmold, C.J.D. Lin, Phys. Rev. D **73**, 014501 (2006). https://doi.org/10.1103/PhysRevD.73.014501
66. V. Braun, D. Müller, Eur. Phys. J. C **55**, 349 (2008). https://doi.org/10.1140/epjc/s10052-008-0608-4
67. A.J. Chambers, R. Horsley, Y. Nakamura, H. Perlt, P.E.L. Rakow, G. Schierholz, A. Schiller, K. Somfleth, R.D. Young, J.M. Zanotti, Phys. Rev. Lett. **118**(24), 242001 (2017). https://doi.org/10.1103/PhysRevLett.118.242001
68. W. Detmold, I. Kanamori, C.J.D. Lin, S. Mondal, Y. Zhao, PoS Lattice **LATTICE2018**, 106 (2018). https://doi.org/10.22323/1.334.0106
69. A. Hannaford-Gunn, R. Horsley, Y. Nakamura, H. Perlt, P.E.L. Rakow, G. Schierholz, K. Somfleth, H. Stüben, R.D. Young, J.M. Zanotti, PoS Lattice **LATTICE2019**, 278 (2020). https://doi.org/10.22323/1.363.0278
70. R. Horsley, Y. Nakamura, H. Perlt, P.E.L. Rakow, G. Schierholz, K. Somfleth, R.D. Young, J.M. Zanotti, PoS Lattice **LATTICE2019**, 137 (2020). https://doi.org/10.22323/1.363.0137
71. W. Detmold, A.V. Grebe, I. Kanamori, C.J.D. Lin, R.J. Perry, Y. Zhao, Phys. Rev. D **104**(7), 074511 (2021). https://doi.org/10.1103/PhysRevD.104.074511
72. K.F. Liu, S.J. Dong, Phys. Rev. Lett. **72**, 1790 (1994). https://doi.org/10.1103/PhysRevLett.72.1790
73. K.F. Liu, S.J. Dong, T. Draper, D. Leinweber, J.H. Sloan, W. Wilcox, R.M. Woloshyn, Phys. Rev. D **59**, 112001 (1999). https://doi.org/10.1103/PhysRevD.59.112001
74. K.F. Liu, Phys. Rev. D **62**, 074501 (2000). https://doi.org/10.1103/PhysRevD.62.074501
75. K.F. Liu, PoS Lattice **LATTICE2015**, 115 (2016). https://doi.org/10.22323/1.251.0115
76. K.F. Liu, Phys. Rev. D **96**(3), 033001 (2017). https://doi.org/10.1103/PhysRevD.96.033001
77. K.F. Liu, Phys. Rev. D **102**(7), 074502 (2020). https://doi.org/10.1103/PhysRevD.102.074502
78. Y.Q. Ma, J.W. Qiu, Phys. Rev. Lett. **120**(2), 022003 (2018). https://doi.org/10.1103/PhysRevLett.120.022003
79. G.S. Bali et al., Eur. Phys. J. C **78**(3), 217 (2018). https://doi.org/10.1140/epjc/s10052-018-5700-9
80. G.S. Bali, V.M. Braun, B. Gläßle, M. Göckeler, M. Gruber, F. Hutzler, P. Korcyl, A. Schäfer, P. Wein, J.H. Zhang, Phys. Rev. D **98**(9), 094507 (2018). https://doi.org/10.1103/PhysRevD.98.094507
81. B. Joó, J. Karpie, K. Orginos, A.V. Radyushkin, D.G. Richards, S. Zafeiropoulos, Phys. Rev. Lett. **125**(23), 232003 (2020). https://doi.org/10.1103/PhysRevLett.125.232003
82. R.S. Sufian, J. Karpie, C. Egerer, K. Orginos, J.W. Qiu, D.G. Richards, Phys. Rev. D **99**(7), 074507 (2019). https://doi.org/10.1103/PhysRevD.99.074507
83. R.S. Sufian, C. Egerer, J. Karpie, R.G. Edwards, B. Joó, Y.Q. Ma, K. Orginos, J.W. Qiu, D.G. Richards, Phys. Rev. D **102**(5), 054508 (2020). https://doi.org/10.1103/PhysRevD.102.054508
84. A.V. Radyushkin, Phys. Rev. D **96**(3), 034025 (2017). https://doi.org/10.1103/PhysRevD.96.034025
85. I. Balitsky, W. Morris, A. Radyushkin, Phys. Lett. B **808**, 135621 (2020). https://doi.org/10.1016/j.physletb.2020.135621
86. K. Orginos, A. Radyushkin, J. Karpie, S. Zafeiropoulos, Phys. Rev. D **96**(9), 094503 (2017). https://doi.org/10.1103/PhysRevD.96.094503
87. J. Karpie, K. Orginos, A. Radyushkin, S. Zafeiropoulos, EPJ Web Conf. **175**, 06032 (2018). https://doi.org/10.1051/epjconf/201817506032
88. J. Karpie, K. Orginos, S. Zafeiropoulos, JHEP **11**, 178 (2018). https://doi.org/10.1007/JHEP11(2018)178
89. J. Karpie, K. Orginos, A. Rothkopf, S. Zafeiropoulos, JHEP **04**, 057 (2019). https://doi.org/10.1007/JHEP04(2019)057
90. B. Joó, J. Karpie, K. Orginos, A. Radyushkin, D. Richards, S. Zafeiropoulos, JHEP **12**, 081 (2019). https://doi.org/10.1007/JHEP12(2019)081
91. B. Joó, J. Karpie, K. Orginos, A.V. Radyushkin, D.G. Richards, R.S. Sufian, S. Zafeiropoulos, Phys. Rev. D **100**(11), 114512 (2019). https://doi.org/10.1103/PhysRevD.100.114512
92. A. Radyushkin, Phys. Rev. D **98**(1), 014019 (2018). https://doi.org/10.1103/PhysRevD.98.014019
93. J.H. Zhang, J.W. Chen, C. Monahan, Phys. Rev. D **97**(7), 074508 (2018). https://doi.org/10.1103/PhysRevD.97.074508
94. T. Izubuchi, X. Ji, L. Jin, I.W. Stewart, Y. Zhao, Phys. Rev. D **98**(5), 056004 (2018). https://doi.org/10.1103/PhysRevD.98.056004
95. M. Bhat, K. Cichy, M. Constantinou, A. Scapellato, Phys. Rev. D **103**(3), 034510 (2021). https://doi.org/10.1103/PhysRevD.103.034510
96. Z. Fan, R. Zhang, H.W. Lin, Int. J. Mod. Phys. A **36**(13), 2150080 (2021). https://doi.org/10.1142/S0217751X21500809
97. R.S. Sufian, T. Liu, A. Paul, Phys. Rev. D **103**(3), 036007 (2021). https://doi.org/10.1103/PhysRevD.103.036007
98. N. Karthik, Phys. Rev. D **103**(7), 074512 (2021). https://doi.org/10.1103/PhysRevD.103.074512
99. T. Khan et al., Phys. Rev. D **104**(9), 094516 (2021). https://doi.org/10.1103/PhysRevD.104.094516
100. Z. Fan, H.W. Lin, Phys. Lett. B **823**, 136778 (2021). https://doi.org/10.1016/j.physletb.2021.136778
101. C. Egerer et al., Phys. Rev. D **106**(9), 094511 (2022). https://doi.org/10.1103/PhysRevD.106.094511
102. A. Salas-Chavira, Z. Fan, H.W. Lin, Phys. Rev. D **106**(9), 094510 (2022). https://doi.org/10.1103/PhysRevD.106.094510
103. Z. Fan, W. Good, H.W. Lin (2022)
104. J. Karpie, K. Orginos, A. Radyushkin, S. Zafeiropoulos, JHEP **11**, 024 (2021). https://doi.org/10.1007/JHEP11(2021)024
105. R. Zhang, C. Honkala, H.W. Lin, J.W. Chen, Phys. Rev. D **102**(9), 094519 (2020). https://doi.org/10.1103/PhysRevD.102.094519
106. X. Gao, A.D. Hanlon, N. Karthik, S. Mukherjee, P. Petreczky, P. Scior, S. Shi, S. Syritsyn, Y. Zhao, K. Zhou, Phys. Rev. D **106**(11), 114510 (2022). https://doi.org/10.1103/PhysRevD.106.114510
107. X. Xiong, X. Ji, J.H. Zhang, Y. Zhao, Phys. Rev. D **90**(1), 014051 (2014). https://doi.org/10.1103/PhysRevD.90.014051
108. Y.Q. Ma, J.W. Qiu, Phys. Rev. D **98**(7), 074021 (2018). https://doi.org/10.1103/PhysRevD.98.074021

109. X. Ji, Y.S. Liu, Y. Liu, J.H. Zhang, Y. Zhao, Rev. Mod. Phys. **93**(3), 035005 (2021). https://doi.org/10.1103/RevModPhys.93.035005
110. X. Gao, A.D. Hanlon, S. Mukherjee, P. Petreczky, P. Scior, S. Syritsyn, Y. Zhao, Phys. Rev. Lett. **128**(14), 142003 (2022). https://doi.org/10.1103/PhysRevLett.128.142003
111. L.B. Chen, W. Wang, R. Zhu, Phys. Rev. Lett. **126**(7), 072002 (2021). https://doi.org/10.1103/PhysRevLett.126.072002
112. M. Constantinou, et al., (2022)
113. S. Chatrchyan et al., Science **338**, 1569 (2012). https://doi.org/10.1126/science.1230816
114. R. Kogler et al., Rev. Mod. Phys. **91**(4), 045003 (2019). https://doi.org/10.1103/RevModPhys.91.045003
115. J. Mammei, S. Riordan, K. Kumar, J. Wexler, K. Paschke, G. Cates, M. Dalton, X. Zheng, P. Souder, R. Holmes, et al
116. E. Moffat, W. Melnitchouk, T.C. Rogers, N. Sato, Phys. Rev. D **104**(1), 016015 (2021). https://doi.org/10.1103/PhysRevD.104.016015
117. T.J. Hou, H.W. Lin, M. Yan, C.P. Yuan (2022)
118. X. Ji, Y. Liu, A. Schäfer, W. Wang, Y.B. Yang, J.H. Zhang, Y. Zhao, Nucl. Phys. B **964**, 115311 (2021). https://doi.org/10.1016/j.nuclphysb.2021.115311
119. D. Stump, J. Pumplin, R. Brock, D. Casey, J. Huston, J. Kalk, H.L. Lai, W.K. Tung, Phys. Rev. D **65**, 014012 (2001). https://doi.org/10.1103/PhysRevD.65.014012
120. M. Aaboud et al., Eur. Phys. J. C **77**(6), 367 (2017). https://doi.org/10.1140/epjc/s10052-017-4911-9
121. J. Pumplin, D.R. Stump, J. Huston, H.L. Lai, P.M. Nadolsky, W.K. Tung, JHEP **07**, 012 (2002). https://doi.org/10.1088/1126-6708/2002/07/012
122. X.D. Ji, Phys. Rev. Lett. **78**, 610 (1997). https://doi.org/10.1103/PhysRevLett.78.610
123. G. Wang, J. Liang, T. Draper, K.F. Liu, Y.B. Yang, Phys. Rev. D **104**, 074502 (2021). https://doi.org/10.1103/PhysRevD.104.074502
124. X. Gao, N. Karthik, S. Mukherjee, P. Petreczky, S. Syritsyn, Y. Zhao, Phys. Rev. D **104**(11), 114515 (2021). https://doi.org/10.1103/PhysRevD.104.114515
125. G.M. Huber et al., Phys. Rev. C **78**, 045203 (2008). https://doi.org/10.1103/PhysRevC.78.045203
126. H.P. Blok et al., Phys. Rev. C **78**, 045202 (2008). https://doi.org/10.1103/PhysRevC.78.045202
127. T. Horn et al., Phys. Rev. C **78**, 058201 (2008). https://doi.org/10.1103/PhysRevC.78.058201
128. T. Horn et al., Phys. Rev. Lett. **97**, 192001 (2006). https://doi.org/10.1103/PhysRevLett.97.192001
129. J. Volmer et al., Phys. Rev. Lett. **86**, 1713 (2001). https://doi.org/10.1103/PhysRevLett.86.1713
130. S.R. Amendolia et al., Nucl. Phys. B **277**, 168 (1986). https://doi.org/10.1016/0550-3213(86)90437-2
131. M. Burkardt, Int. J. Mod. Phys. A **18**, 173 (2003). https://doi.org/10.1142/S0217751X03012370
132. M. Diehl, Phys. Rept. **388**, 41 (2003). https://doi.org/10.1016/j.physrep.2003.08.002